# Visible light responsive heterostructure HTDMA-$BiPO_4$ modified clays for effective diclofenac oxidation: role of interface interactions and basal spacing

*Imen Fellah[1], Ridha Djellabi[2,*], Hédi Ben Amor[1], Nesrine Abderrahim[1], Claudia L. Bianchi[2], Alessia Giordana[3], Giuseppina Cerrato[3], Noureddine Hamdi[4]*

[1]*Engineering school (ENIG), RL Processes, Energetic, Environment and ElectricSystems (PEESE) University of Gabes. Gabes 6072, Tunisia.*

[2]*Department of Chemistry, University of Milan, Via Golgi 19, Milano 20133, Italy*

[3]*University of Gabès, Higher Institute of Sciences and Techniques of Waters, Tunisia.*

[4]*Department of Chemistry, University of Turin, Via Pietro Giuria 7, 10125 Turin, Italy*

## Graphical abstract

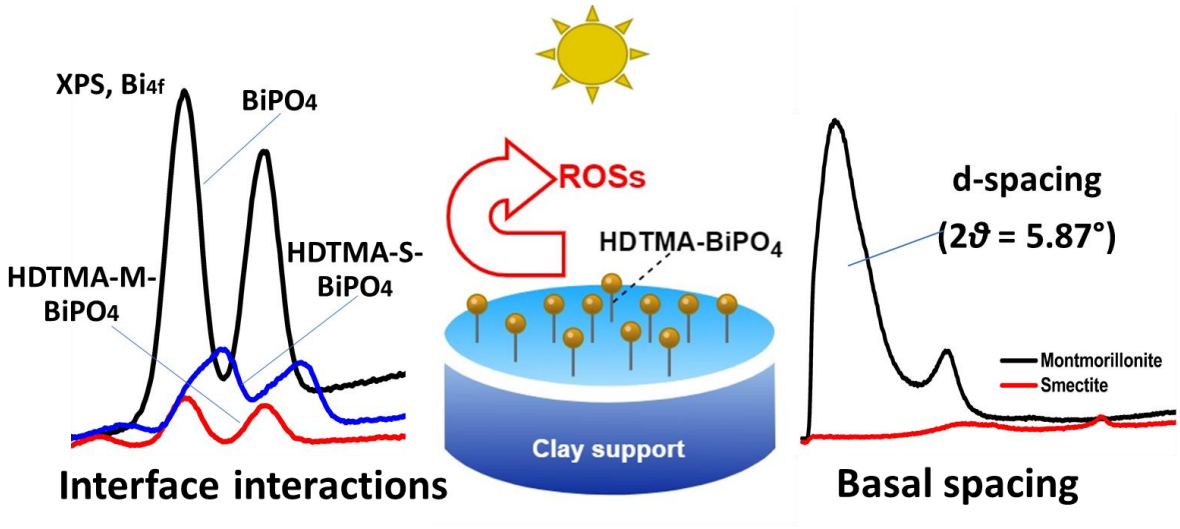

**Abstract,**

In the present study, we investigated comparatively the role of hexadecyltrimethylammonium bromide (HDTMA) in enhancing the adsorption and photocatalytic activity of $BiPO_4$ coated Montmorillonite (M-$BiPO_4$), and $BiPO_4$ coated smectite (S-$BiPO_4$). Firstly, the direct hybridization of $BiPO_4$ with clays results in enhanced adsorption and photocatalytic efficiency for the oxidation of diclofenac under solar light compared to bare $BiPO_4$. Due to the different interlayer spacing of montmorillonite (big) and smectite (small), the hybridization of both $BiPO_4$ and HDTMA on the surface of clays led to different mechanistic pathways. In terms of montmorillonite, the insertion of $BiPO_4$ and HDTMA can be realized between the interlayer, while in the case of the smectite, they might be fixed on the external surface. HDTMA reacts better with $BiPO_4$ set on the external surface to form better heterostructure, as proved by XPS analysis. No peak shifting was observed in $Bi_{4f}$ high resolution in HDTMA-M-$BiPO_4$, while a strong shift by 1.3 eV along with an obvious change in the shape of peaks was noticed in HDTMA-S-$BiPO_4$. In addition, the $P_{2p}$ profiles show a positive peak shifting by around 0.7 and 3 eV for HDTMA-M-$BiPO_4$ and HDTMA-S-$BiPO_4$, respectively. Regarding the adsorption and photocatalytic tests, at lower concentration (20 ppm), M-$BiPO_4$ was several times more effective than S-$BiPO_4$. However, the coating of clays by $BiPO_4$ and HDTMA showed a different manner, wherein HDTMA-S-$BiPO_4$ achieved an oxidation rate of around 88% under solar light within 90 min at a concentration of 140 ppm of diclofenac. On the contrary, HDTMA-M-$BiPO_4$ shows an oxidation rate of only 22 % under the same conditions. It was deduced that the strong surface interactions between HDTMA and $BiPO_4$ coated on smectite can form a strong interfacial bridge which boosts the visible light response and the separation of photogenerated charges.

**Keywords:** Interfacial interaction, HDTMA-$BiPO_4$, Heterostructures, Solar photocatalysis, Water remediation.

## Introduction

$TiO_2$ photocatalysis, since it is discovered in 1972 by Fujishima and Honda [1], has passed by extensive fundamental research and technology pathways towards environmental remediation and energy production [2-6]. The photocatalytic materials fabrication side has taken the most of such scientific and technological research advancements, and many types of photocatalytic materials have been suggested within the last decades [7-12]. Even with such a pool of reported research over more than 30 years, photocatalytic technology is still not convincing enough to be applied extensively in real-world due to many technological and economic issues. Shortly, to convince the scientific community to invest in photocatalytic technology, several issues should be pointed out, including the efficiency of the photocatalytic system compared to existing technologies for a given application, the cost and sustainability of the system. In terms of water purification via the photocatalytic process, many benefits and weaknesses have been raised recently, putting the photocatalytic technology under huge criticisms. Advantages of photocatalysis can involve using solar light as a free energy resource to purify the water on sunny days/regions in a quasi-continuous economic way. However, a correct application should be found to use photocatalysis since this technology is applicable under limited conditions (i.e., less dense wastewaters) because of the use of light to activate the photocatalysts. Based on the reported research, photocatalytic technology has shown low mass transfer (primarily when naked semiconductors are used), generation of by-products, surface deactivation, and complicated or/and expensive synthesis of materials, and so on, as discussed recently by Djellabi et al. [13]. For better technology transfer, several approaches have been suggested to overcome such drawbacks. One of them, the combination of photocatalytic semiconductors with highly adsorptive materials, has been considered as a successful approach. In such a combination, several unique characteristics can be obtained as follows: (i): the coating of small nanoparticles (NPs) of semiconductors on the large particle of adsorbent solves the problem of hard recovery of NPs after the treatment. (ii): The photocatalytic action of NPs on the surface of adsorbent can limit the fast

saturation since the oxidative by photogenerated reactive oxygen species (ROSs) reduces the content of pollutants and liberates different adsorptive sites. (iii): Unlike naked semiconductors, the photogenerated by-products can be adsorbed on the surface for further oxidation, avoiding their toxicity in water. (iv): visible light response of semiconductors can be improved when they are hybridized with some adsorptive materials due to the photosensitizing or surface interactions [14, 15]. Synergism between the photocatalytic activity and the adsorption effect can be found, wherein a cooperative mechanism, so-called Adsorb and Shuttle process, can take place to remove the pollutants even at higher concentrations [16, 17].

Bismuth phosphate ($BiPO_4$), a relatively newly emerging photocatalyst, which was used for the first time in 2010 [18], has been reported to be very effective towards the oxidation of organic pollutants due to its more positive valance band compared to the common $TiO_2$, allowing better oxidation of water molecules into a high yield of hydroxyl radicals. However, $BiPO_4$ exhibits a large bandgap (in the range of 3.5–4.6 eV), and it requires a strong UV light irradiation to be activated. Loeb *et al.* reported in their critical review [19] that $BiPO_4$ could be a great alternative photocatalyst for the oxidation and mineralization of organic pollutants. At the same time, creative and yet-to-be-devised approaches to fix its drawbacks are needed to benefit from this promising photocatalyst for its use in photocatalytic wastewater treatment. Several approaches have been already reported to enhance the adsorption ability and visible light response of $BiPO_4$ such as doping [20-22], heterojunction systems [23-25], oxygen vacancy [26-29], phase junction [30-32], and combination with π–conjugated materials [33-35].

In the present work, the enhancement of the ability of $BiPO_4$ was carried out via the hybridization with two clays (smectite and montmorillonite) to enhance its adsorption capacity and photoactivity under UV and solar light towards the oxidation of diclofenac. To further improve the performance of $BiPO_4$-clay based photocatalysts, hexadecyl trimethyl ammonium bromide (HDTMA) was used to modify the clay before the coating of $BiPO_4$. The role of HDTMA in enhancing the adsorption and

photocatalytic abilities was investigated. Finally, the optimization of $BiPO_4$ amount coated on the surface HDTMA modified smectite was studied to figure out the ratio of $BiPO_4$ towards the adsorption and photoactivity.

## 2. Materials and methods

### 2.1. Synthesis of photocatalysts

The raw montmorillonite used in this study was obtained from Roussel deposit in Maghnia (Algeria). Its cationic exchange capacity is 89.30 mmol/100 g. The raw smectite is gray clay derived from Djebel haidoudi near El hamma, and it exhibits a cation exchange capacity of 64.28 meq/100 g. The fabrication of Montmorillonite-$BiPO_4$ (M- $BiPO_4$) was carried out by simple precipitation of $BiNO_3$ and $NaH_2PO_4$ on the surface of Montmorillonite. For this purpose, 1 g of montmorillonite is spread in 20 mL ultrapure water and sonicated for 20 min. Then, under stirring, 5 mL of $BiNO_3$ (0.3 M) is added dropwise into montmorillonite mixture and left for 60 min under stirring at 60°C. After that, 5 mL of $NaH_2PO_4$ (0.3 M) is added dropwise into the mixture, and stirred for 2 h. The obtained solid was washed and dried at 120°C for a night. HTDMA-Montmorillonite (HTDMA-M) and HTDMA-smectite (HTDMA-S) were prepared by adding a desired amount of HTDMA to water-montmorillonite or smectite, followed by microwave treatment. The sample was recovered and dried at 120 for a night. HTDMA-M-$BiPO_4$ and HTDMA-S-$BiPO_4$ were prepared by precipitation of $BiNO_3$ and $NaH_2PO_4$ as described above. Bare $BiPO_4$ was also prepared for the comparison.

### 2.2. Characterization

Fourier transform infrared spectroscopy analyses (FT-IR) analysis on the as-prepared samples was carried out using a Bruker Vertex 70 spectrophotometer (Bruker, Billerica, MA, US). XRD spectra of samples were recorded on a PANalytical X'PERT-PRO diffractometer with monochromatic CuKα radiation (λ = 1.54056 Å). X-ray photoelectron spectra (XPS) were recorded on a XPS PHI Quantum

instrument. UV–Vis absorption spectra were recorded in the wavelength range of 300–800 nm on Cary 5000 UV-Vis spectrophotometer (Agilent Technology).

### 2.3. Adsorption and photocatalytic tests

The efficiency of as-prepared photocatalysts was tested against the photocatalytic oxidation of diclofenac under UV ($\lambda_{max}$ = 365 nm, 100 W/m$^2$) and solar light (35 W·m$^{-2}$, ULTRA VITALUX 300 W-OSRAM, OSRAM, Múnich, Germany) irradiations. Dark and photolysis experiments were carried out for the purpose of comparison. At different time intervals, samples were collected and filtered using filter paper of 0.45 μm diameter. The analysis of diclofenac was performed using a UV-vis spectrophotometer at a wavelength of 276 nm.

## 3. Results and discussion

### 3.1. Characterization of materials

XRD patterns of $BiPO_4$, M, M-$BiPO_4$, HDTMA-M-$BiPO_4$, S, S-$BiPO_4$ and HDTMA-M-$BiPO_4$ samples are shown in **Figure 1**. In $BiPO_4$ and all $BiPO_4$ modified clays, diffraction peaks were appeared at around 14.7, 20.1, 25.5, 29.5, 31.3, 41.9, and 48.7° which fit with the crystal orientations of the hexagonal phase of $BiPO_4$ (space group: P3121(152), JCPDS, card no. 15-0766) [36]. Montmorillonite's XRD pattern shows a strong d(100) basal spacing reflection at around $2\theta$ = 5.87° [37]. However, after the coating of $BiPO_4$ on the surface of M, this peak was reduced significantly, confirming the formation of $BiPO_4$ nanoparticles between the montmorillonite layers. The bare smectite pattern does not show a strong basal spacing diffraction peak compared to the montmorillonite sample. The coating of $BiPO_4$ on HDTMA modified clays resulted in stronger intensities of $BiPO_4$ diffraction peaks. This may be due to the better crystallization and distribution of $BiPO_4$ nanoparticles on the surface of HDTMA-clays. The HDTMA organic fragments can interact between the layers of the clay, and also it may react with the components of the clay on the external surface. It may be deduced that the clays with larger basal spacing can receive HDTMA organic fragments compared to those with lower basal spacing. Therefore, the introduction of $BiPO_4$ on

144 HDTMA modified clays having different basal spacing could have different manners. It is expected
145 that the $BiPO_4$ could be accumulated in the basal spacing of montmorillonite, while $BiPO_4$ might be
146 mostly coated on the external surface of smectite because of its low basal spacing.

147 **Figure 2** shows FTIR curves of different samples. In bare $BiPO_4$, the large band at 750-1200 $cm^{-1}$ is
148 assigned to the characteristic asymmetric stretching modes of P–O bonds of $PO_4^{3-}$ [38]. Peaks at the
149 range 520-600 $cm^{-1}$ are due to the bending vibrations of O–P–O linkage. Characteristic peaks of
150 $BiPO_4$ were not very obvious in $BiPO_4$ modified clay samples, which could be overlapped with the
151 original peaks since both montmorillonite and smectite clays have absorption peaks at the same area,
152 i.e., the band at around 1000 $cm^{-1}$ and around 600 $cm^{-1}$ is due to Si-O stretching in-plane and Al-O-
153 Si deformation, respectively [37, 39]. FTIR confirmed the fixation of HTDMA in HDTMA-M-$BiPO_4$,
154 S, S-$BiPO_4$, and HDTMA-M-$BiPO_4$ samples curves, wherein two peaks at around 2936 and 2871 $cm^{-1}$
155 were appeared due to the presence of $CH_2$ and $CH_3$, respectively [40].

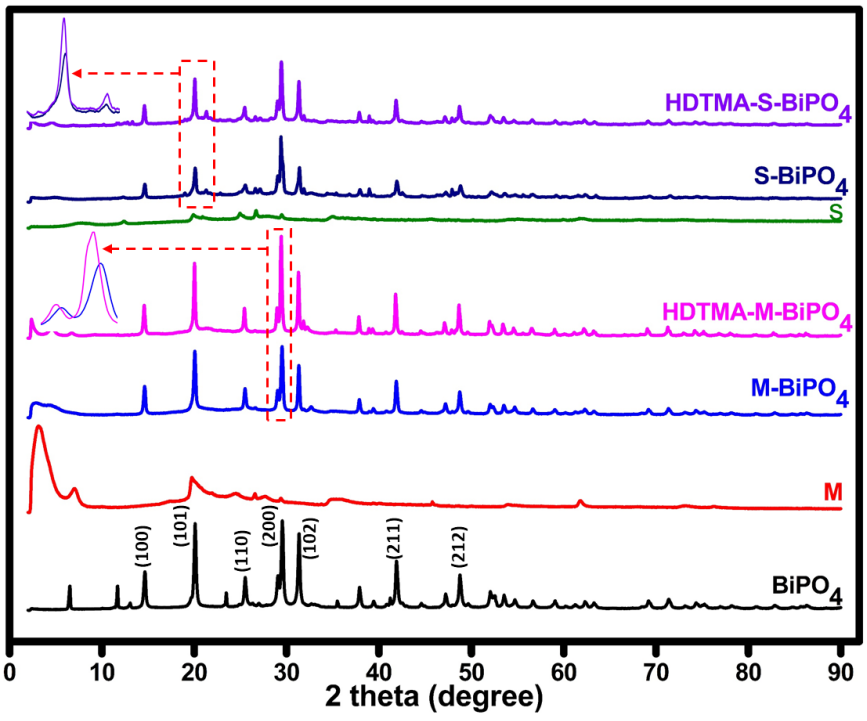

156

157 **Figure 1**. XRD patterns of $BiPO_4$, M, M-$BiPO_4$, HDTMA-M-$BiPO_4$, S, S-$BiPO_4$ and HDTMA-S-
158 $BiPO_4$ samples.

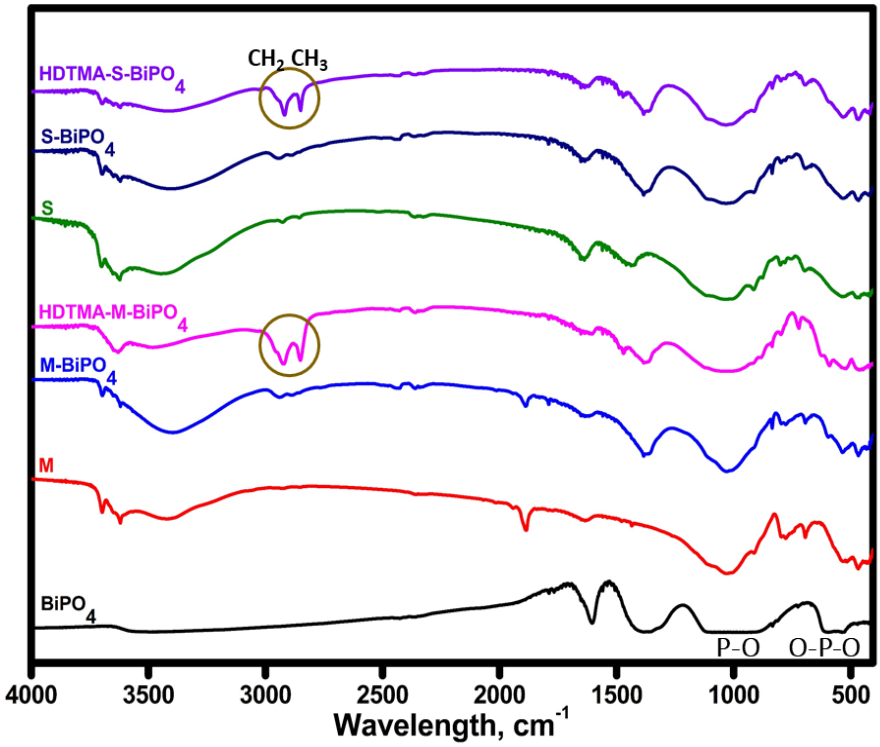


**Figure 2**. FTIR spectra of $BiPO_4$, M, M-$BiPO_4$, HDTMA-M-$BiPO_4$, S, S-$BiPO_4$ and HDTMA-S-$BiPO_4$ samples.

The results of XPS analysis carried out on $BiPO_4$, HDTMA-M-$BiPO_4$, and HDTMA-S-$BiPO_4$ samples are shown in **Figure 3**. In terms of $Bi_{4f}$ high resolution (**Figure 3,b**), $BiPO_4$ profile shows two intense peaks at 159.5 and 164.9 eV, which are due to $Bi_{4f7/2}$ and $Bi_{4f5/2}$, respectively, showing the trivalent oxidation state of Bi species [41]. The distance between $Bi_{4f7/2}$ and $Bi_{4f5/2}$ was calculated to be 5.3 eV. The position of these peaks was not affected in the case of HDTMA-M-$BiPO_4$, but a significant change in the intensity is observed because of the low quantity of $BiPO_4$. In the case of HDTMA-S-$BiPO_4$, a huge change in $Bi_{4f}$ peaks was recorded. The shape of peaks was deformed along with a significant shift towards higher binding energies. The peaks shifting was about 1.3 eV, while the distance between $Bi_{4f7/2}$ and $Bi_{4f5/2}$ was reduced to 5.3 eV. Such a change proves the strong interactions between the atoms of $BiPO_4$ and the components of HDTMA-S. **Figure 3,c** shows $O_{1s}$ profiles in $BiPO_4$, HDTMA-M-$BiPO_4$ and HDTMA-S-$BiPO_4$. Bare $BiPO_4$ shows a single peak at 532.2 eV assigned to crystalline oxygen [42]. $O_{1s}$ spectra in HDTMA-M-$BiPO_4$ and HDTMA-S-

$BiPO_4$ show a significant shifting towards higher binding energies by around 1.8 and 3.1 eV, respectively, which might be due to the adsorbed oxygen and the chemical interactions between crystalline $O^{2-}$ of $BiPO_4$ and HDTMA-clay supports. The $P_{2p}$ of $PO_4^{3-}$ state was appeared at a binding energy of 132.8 eV in bare $BiPO_4$ [43], while a notable shift towards higher energies by 0.7 and 3 eV was detected in HDTMA-M-$BiPO_4$ and HDTMA-S-$BiPO_4$ samples, respectively. The observed peaks shifting in HDTMA-M-$BiPO_4$ and HDTMA-S-$BiPO_4$ reflects the migration of electron density of $BiPO_4$ to HDTMA-clay components and the formation of a built-in electric field at the interface. It is important to point out that the XPS peak shifting in HDTMA-S-$BiPO_4$ is more evident than HDTMA-M-$BiPO_4$, suggesting that the characteristics of clays play an important role in forming the surface interactions. In fact, from XRD patterns, it can be seen that M samples exhibit a strong interlayer d-spacing ($2\theta$ = 5.87°), wherein, $BiPO_4$ particles can be introduced and fixed inside the interlayers, as confirmed by the XRD pattern of M-$BiPO_4$ (significant reduction $2\theta$ = 5.87° in peak). However, in terms of the S sample, BiPO4 might be fixed on the external surface due to the low interlayer spacing, which allows the interaction with the added HDTMA to form more interactions and heterostructure. The optical properties of samples were estimated by UV–Vis diffuse reflectance (Figure 4). Respect to bare $BiPO_4$, all samples showed a red-shift in the absorption edge. The band gaps of $BiPO_4$, HDTMA-S-$BiPO_4$ and HDTMA-M-$BiPO_4$ were estimated about 3.87, 2.75 and 2.60 eV, respectively. Interestingly, samples with HDTMA showed as well an ulterior peak centrated at around 380 nm which proves the formation of heterojunction system that would boost further the absorption of light and the photosensitization effect.

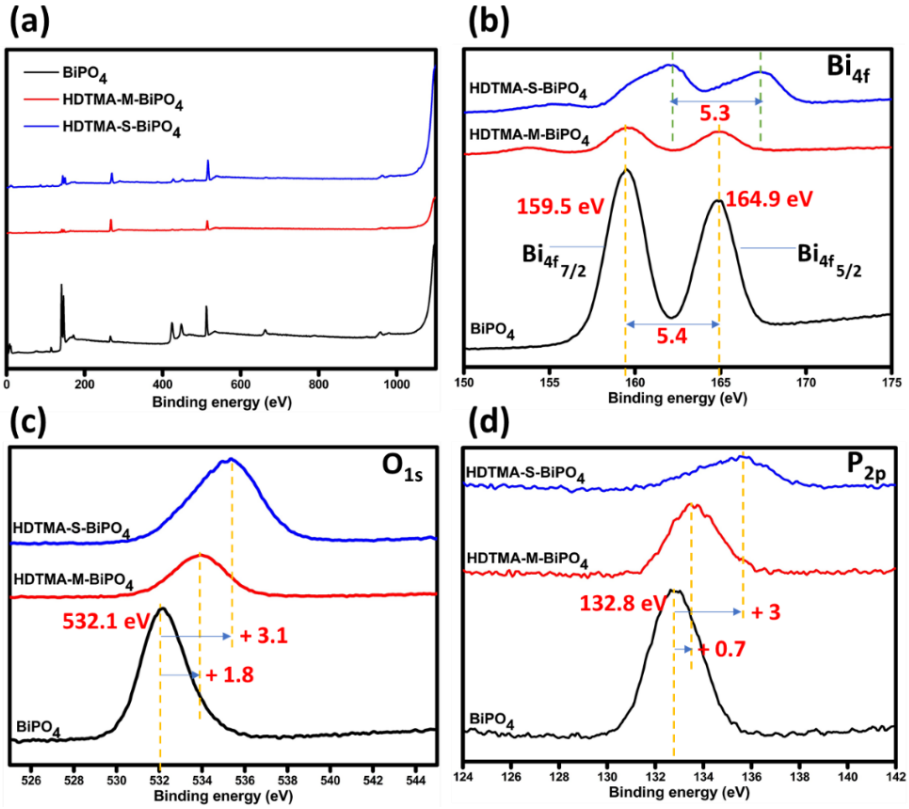


**Figure 3**. (a): XPS survey spectra of $BiPO_4$, HDTMA-M-$BiPO_4$, and HDTMA-S-$BiPO_4$ samples. (b): Bi4f high-resolution profiles. (c): O1s high-resolution profiles. (d): $P_{2P}$ high-resolution profiles.

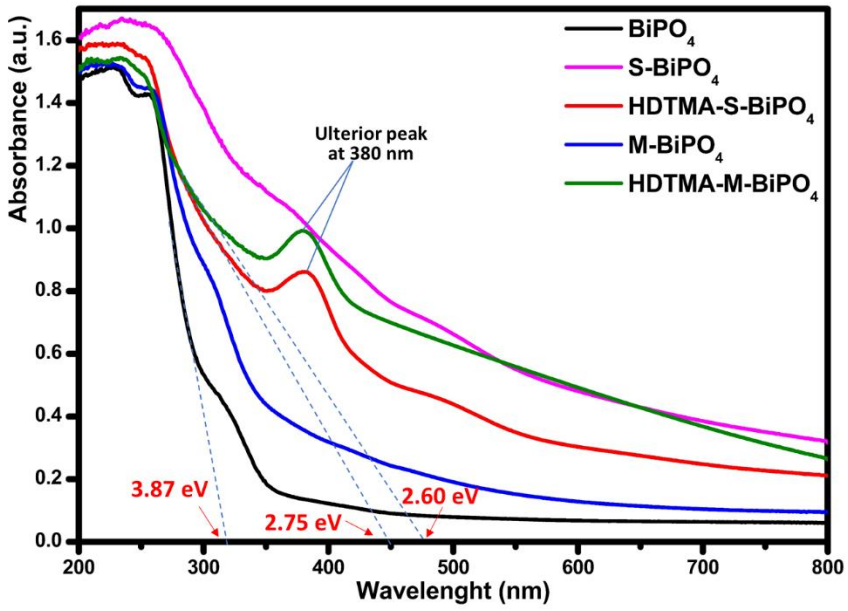


**Figure 4.** UV–Vis diffuse reflectance spectra of bare $BiPO_4$, S-$BiPO_4$, HDTMA-S-$BiPO_4$, M-$BiPO_4$ and HDTMA-M-$BiPO_4$.

### 3.2. Photocatalytic activity

The adsorption and photoactivity of bare $BiPO_4$ and M-$BiPO_4$ under LED, UV, and solar light were tested comparatively, and the results are shown in **Figure 5**. From **Figure 5.a**, it can be noticed that the coating of $BiPO_4$ on the M surface led to enhanced adsorption ability compared to bare M and $BiPO_4$, which could be due to the formation of novel surface adsorption sites. Under LED light irradiation (**Figure 5.b**), no photocatalytic activity was observed using bare $BiPO_4$, while it can be seen that M- $BiPO_4$ has a slight photocatalytic activity under light. It is expected that bare $BiPO_4$ is not photoactive under visible light due to its large bandgap. However, its hybridization with the montmorillonite by in situ precipitation might light to form chemical interactions with the components, as shown in XPS spectra. Under UV light (**Figure 5. c**), bare $BiPO_4$ shows a modest photocatalytic activity, wherein less than 40 % diclofenac was removed. On the other hand, M-$BiPO_4$ shows much better photocatalytic oxidation under UV light of diclofenac, more than 80 % within 90 min. The reasons behind the enhanced removal of diclofenac under UV is undoubtedly due to the combination of adsorption and photocatalytic activity in the same platform, wherein the adsorb & and shuttle process can accelerate the photooxidation of diclofenac. The adsorptive domain (M) acts to concentrate the diclofenac molecules on the surface nearby the photoactive $BiPO_4$, resulting in fast oxidation by photogenerated ROSs [16]. Indeed, the bridge between the surface of M and $BiPO_4$ might help to enhance the generation of ROSs due to the better e-/h+ charges separation. Remarkably, M- $BiPO_4$ showed excellent photoactivity under solar light, which could be due to the self-doping of $BiPO_4$ or structure modification during the precipitation of $BiPO_4$ on the surface of M. Bonds between $BiPO_4$ and M might lead to decrease the bandgap and promotes the charge generation and separation.

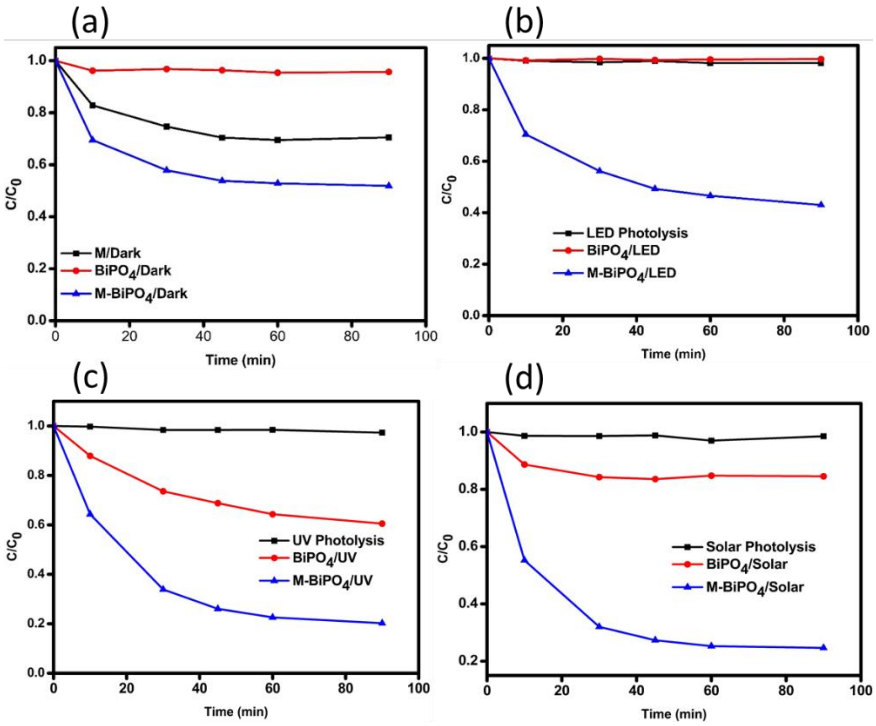


**Figure 5**. (a): Adsorption of diclofenac by bare M, $BiPO_4$, and M- $BiPO_4$, (b): photolysis and photocatalytic oxidation of diclofenac under LED irradiation by $BiPO_4$ and M- $BiPO_4$, (c): photolysis and photocatalytic oxidation of diclofenac under UV irradiation by $BiPO_4$ and M- $BiPO_4$, (d): photolysis and photocatalytic oxidation of diclofenac under solar irradiation by $BiPO_4$ and M- $BiPO_4$. [Photocatalyst]: 0.5 g/L, [Diclofenac]: 20 ppm.

To further evaluate the adsorption/photocatalytic synergism in M-$BiPO_4$ photocatalyst, adsorption and solar photocatalytic experiments were carried out with different diclofenac concentrations and different M-$BiPO_4$ masses. As depicted in **Figure 6.a**, at lower concentrations, the adsorption process is predominant compared to the photocatalytic oxidation. The more the diclofenac concentration is, the more photocatalytic oxidation is evident. At concentrations of 40 and 50 ppm, the removal of diclofenac by photocatalytic effect is pronounced. The behavior of the M-$BiPO_4$ at different masses (**Figure 6.b**) shows that the more the mass of photocatalyst is, the more adsorption of diclofenac is obtained. It is important to mention that the photocatalytic effect, in such a type of materials, has another advantage compared to simple adsorption, which is the self-cleaning of the surface for further adsorption, which in turn retards the fast saturation of the material.

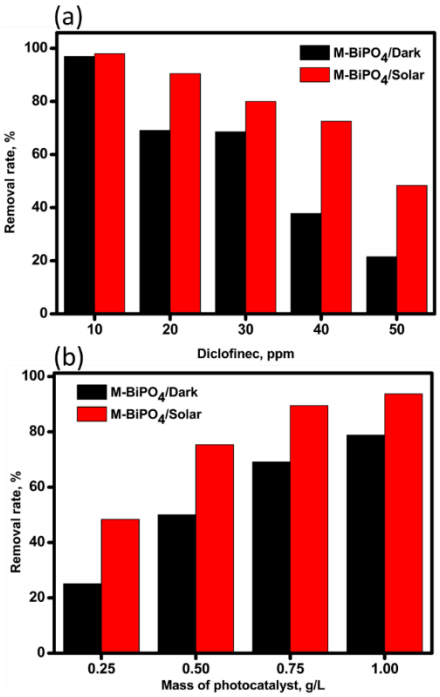


**Figure 6**. (a): Effect of diclofenac concentration on the adsorption and photocatalytic activity under solar light. [Photocatalyst]: 0.75 g/L, contact time 90 min. (b): Effect of photocatalyst mass on the removal of diclofenac by adsorption and photocatalytic activity under solar light, [diclofenac]: 20 ppm, contact time 90 min.

To investigate the role of HDTMA and the type of clay support, HDTMA-M-$BiPO_4$ and HDTMA-S-$BiPO_4$ were fabricated, and their photocatalytic activities were evaluated at different diclofenac concentrations ranging from 50 ppm to 140 ppm (**Figure 7**). Firstly, the photocatalytic tests showed that M-$BiPO_4$ exhibits higher photocatalytic activity under solar light compared to S-$BiPO_4$ at a concentration of 50 ppm. In this case, M-$BiPO_4$ might have better porosity and photoactivity as compared to the S-$BiPO_4$ sample. The fixation of $BiPO_4$ on the montmorillonite, which has an excellent basal spacing, allows a better distribution of $BiPO_4$ particles. It can be seen in XRD patterns (**Figure 1**) that the peaks in M-$BiPO_4$ are more intense than those in S-$BiPO_4$. In addition, since M-$BiPO_4$ has better adsorption ability, a higher photoactivity is expected by adsorb and shuttle means [44, 45]. However, the introduction of HDTMA to the surface of montmorillonite and smectite before the coating of $BiPO_4$ has changed the manner completely. In terms of HDTMA-M-$BiPO_4$, the

adsorption ability of the composite was significantly enhanced, leading to faster removal of diclofenac. It can also be seen that the adsorption is predominant in the photocatalytic action in HDTMA-M-$BiPO_4$ system, especially at a concentration ranging from 50 to 100 ppm. The removal rates decrease as a function of diclofenac concentration. It might be deduced the enhancement in the effectiveness of HDTMA-M-$BiPO_4$ is more due to the adsorb and shuttle process that can be appeared in the platform of this material, which improves the concentration of diclofenac molecules on the surface near the photoactive $BiPO_4$. On top of that, the photocatalytic activity of $BiPO_4$ fixed on the surface of montmorillonite might also be improved through chemical interactions with HDTMA. In the case of HDTMA-S-$BiPO_4$, another surprising manner was found. HDTMA has notably enhanced the adsorption ability of the composite, but it has a major role for photocatalytic activity under solar light. The removal of diclofenac under solar light was high even at higher concentrations, by photocatalytic means as a predominant action, unlike HDTMA-S-$BiPO_4$. Based on these results and XPS analysis, it might be deduced that the photocatalytic activity in HDTMA-S-$BiPO_4$ under solar light is assigned to the strong interface interactions between $BiPO_4$ and HDTMA, forming a heterostructure platform. A better visible light response and an enhanced photoproduced charges separation can be found in the HDTMA-S-$BiPO_4$ surface because of the interface junction. As a result, a higher yield of reactive oxygen species can be produced in the medium. $BiPO_4$ is an excellent producer of hydroxyl radicals, compared to common photocatalysts (i.e., $TiO_2$), because of its more positive valance band. However, this photocatalyst requires surface modification to decrease its bandgap and improve the separation of $e^-/h^+$ charge carriers. Interestingly, the hybridization of $BiPO_4$ and HDTMA in our conditions had solved perfectly such structure drawbacks.

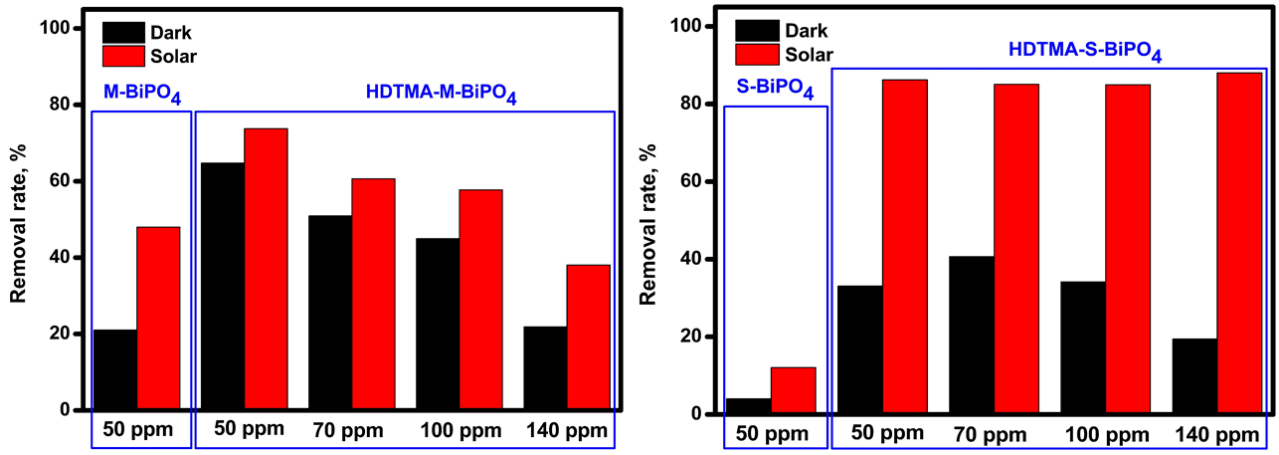


**Figure 7**. Adsorption and photocatalytic oxidation of diclofenac by $BiPO_4$ modified clays and $BiPO_4$ modified HDTMA-clays, at different diclofenac concentrations. [Photocatalyst]: 0.375 g/L, contact time 90 min.

## 4. Conclusions

The results of this investigation show the significant role of the co-hybridization of $BiPO_4$ and HDTMA on the surface of clays, namely, montmorillonite and smectite. In the first study, it was found out that the coating of $BiPO_4$ on the surface of montmorillonite leads enhanced adsorption and photocatalytic activity for the oxidation of diclofenac under LED, UV, and solar light irradiations. Compared to M- $BiPO_4$, S-$BiPO_4$ was less efficient in adsorption and photocatalytic activity under solar light. Such a difference in the effectiveness might be due to the different basal spacing of the original clay material, having the montmorillonite an extra-large basal spacing compared to smectite. The co-modification of clays by $BiPO_4$ and HDTMA has shown interesting results in terms of interface interactions. HDTMA in HDTMA-M-$BiPO_4$ had a positive effect of improving further the adsorption ability and the photoactivity, wherein diclofenac was removed mostly by physical adsorption. However, in HDTMA-S-$BiPO_4$ composite, HDTMA has enhanced the adsorption ability from one side. Still, mostly HDTMA has improved the photoactivity of BiPO4 dramatically by forming an interfacial bridge, confirmed by XPS analysis, which leads to excellent photoexcitation

293 and separation of charges carries. This study showed promising results in enhancing the adsorption
294 and photoactivity abilities of clay-$BiPO_4$ by sustainable and straightforward surface modification.

295 **References**


296 [1] A. Fujishima, K. Honda, Electrochemical photolysis of water at a semiconductor electrode, nature,
297 238 (1972) 37-38.
298 [2] J. Luo, S. Zhang, M. Sun, L. Yang, S. Luo, J.C. Crittenden, A critical review on energy conversion
299 and environmental remediation of photocatalysts with remodeling crystal lattice, surface, and
300 interface, ACS nano, 13 (2019) 9811-9840.
301 [3] A. Rani, R. Reddy, U. Sharma, P. Mukherjee, P. Mishra, A. Kuila, L.C. Sim, P. Saravanan, A
302 review on the progress of nanostructure materials for energy harnessing and environmental
303 remediation, Journal of Nanostructure in Chemistry, 8 (2018) 255-291.
304 [4] K. Kabra, R. Chaudhary, R.L. Sawhney, Treatment of hazardous organic and inorganic
305 compounds through aqueous-phase photocatalysis: a review, Industrial & engineering chemistry
306 research, 43 (2004) 7683-7696.
307 [5] A.A. Ismail, D.W. Bahnemann, Photochemical splitting of water for hydrogen production by
308 photocatalysis: A review, Solar energy materials and solar cells, 128 (2014) 85-101.
309 [6] K. Perović, M. Kovačić, H. Kušić, U.L. Štangar, F. Fresno, D.D. Dionysiou, A. Loncaric Bozic,
310 Recent achievements in development of TiO2-based composite photocatalytic materials for solar
311 driven water purification and water splitting, Materials, 13 (2020) 1338.
312 [7] R. Djellabi, M.F. Ordonez, F. Conte, E. Falletta, C.L. Bianchi, I. Rossetti, A Review of Advances
313 in Multifunctional XTiO3 Perovskite-type Oxides as piezo-photocatalysts for Environmental
314 Remediation and Energy Production, Journal of Hazardous Materials, (2021) 126792.
315 [8] M.G. Alalm, R. Djellabi, D. Meroni, C. Pirola, C.L. Bianchi, D.C. Boffito, Toward Scaling-Up
316 Photocatalytic Process for Multiphase Environmental Applications, Catalysts, 11 (2021) 562.

317 [9] T. Hisatomi, J. Kubota, K. Domen, Recent advances in semiconductors for photocatalytic and
318 photoelectrochemical water splitting, Chemical Society Reviews, 43 (2014) 7520-7535.
319 [10] C. Xu, P.R. Anusuyadevi, C. Aymonier, R. Luque, S. Marre, Nanostructured materials for
320 photocatalysis, Chemical Society Reviews, 48 (2019) 3868-3902.
321 [11] J. Low, J. Yu, M. Jaroniec, S. Wageh, A.A. Al-Ghamdi, Heterojunction photocatalysts,
322 Advanced materials, 29 (2017) 1601694.
323 [12] R. Djellabi, C.L. Bianchi, M.R. Haider, J. Ali, E. Falletta, M.F. Ordonez, A. Bruni, M. Sartirana,
324 R. Geioushy, Photoactive Polymer for Wastewater Treatment, Nanomaterials for Water Treatment
325 and Remediation, CRC Press2021, pp. 217-244.
326 [13] R. Djellabi, R. Giannantonio, E. Falletta, C.L. Bianchi, SWOT analysis of photocatalytic
327 materials towards large scale environmental remediation, Current Opinion in Chemical Engineering,
328 33 (2021) 100696.
329 [14] R. Djellabi, B. Yang, Y. Wang, X. Cui, X. Zhao, Carbonaceous biomass-titania composites with
330 TiOC bonding bridge for efficient photocatalytic reduction of Cr (VI) under narrow visible light,
331 Chemical Engineering Journal, 366 (2019) 172-180.
332 [15] R. Djellabi, B. Yang, K. Xiao, Y. Gong, D. Cao, H.M.A. Sharif, X. Zhao, C. Zhu, J. Zhang,
333 Unravelling the mechanistic role of TiOC bonding bridge at titania/lignocellulosic biomass interface
334 for Cr (VI) photoreduction under visible light, Journal of colloid and interface science, 553 (2019)
335 409-417.
336 [16] A.N. Saber, R. Djellabi, I. Fellah, N. Abderrahim, C.L. Bianchi, Synergistic sorption/photo-
337 Fenton removal of typical substituted and parent polycyclic aromatic hydrocarbons from coking
338 wastewater over CuO-Montmorillonite, Journal of Water Process Engineering, 44 (2021) 102377.
339 [17] R. Djellabi, M.F. Ghorab, A. Smara, C.L. Bianchi, G. Cerrato, X. Zhao, B. Yang, Titania–
340 Montmorillonite for the photocatalytic removal of contaminants from water: adsorb & shuttle process,
341 Green materials for wastewater treatment, Springer2020, pp. 291-319.

342 [18] C. Pan, Y. Zhu, New type of BiPO4 oxy-acid salt photocatalyst with high photocatalytic activity
343 on degradation of dye, Environmental science & technology, 44 (2010) 5570-5574.
344 [19] SK. Loeb, P.J. Alvarez, J.A. Brame, E.L. Cates, W. Choi, J. Crittenden, D.D. Dionysiou, Q. Li,
345 G. Li-Puma, X. Quan, The technology horizon for photocatalytic water treatment: sunrise or sunset?,
346 ACS Publications, 2018.
347 [20] J. Wang, N. Luo, S. Peng, L. Yang, M. Zhao, BiPO4: Ln3+ (Ln= Eu, Tb, Eu/Tb) nanorods:
348 room-temperature synthesis, reaction mechanism, and color-tunable emission, Journal of Alloys and
349 Compounds, (2021) 162314.
350 [21] Y. Quan, X. Ji, K. Liu, C. Kang, Synthesis, characterization, and photocatalytic properties of La
351 3+-doped BiPO 4 photocatalysts, Kinetics and Catalysis, 57 (2016) 207-211.
352 [22] D. Yu, X. Wu, G. Yan, J. Cao, Crystal phase, morphology evolution and luminescence properties
353 of Eu3+-doped BiPO4 phosphor prepared using the hydrothermal method, Luminescence, (2021).
354 [23] X. Ma, J. Hu, H. He, S. Dong, C. Huang, X. Chen, New understanding on enhanced
355 photocatalytic activity of g-C3N4/BiPO4 heterojunctions by effective interfacial coupling, ACS
356 Applied Nano Materials, 1 (2018) 5507-5515.
357 [24] N. Sun, Y. Qu, C. Yang, Z. Yang, R. Yan, E. Wenyu, Z. Zhang, Z. Li, H. Li, I. Khan, Efficiently
358 photocatalytic degradation of monochlorophenol on in-situ fabricated BiPO4/β-Bi2O3 heterojunction
359 microspheres and O2-free hole-induced selective dechloridation conversion with H2 evolution,
360 Applied Catalysis B: Environmental, 263 (2020) 118313.
361 [25] M. Yuan, T. Liu, Q. Shi, J. Dong, Understanding the KOH activation mechanism of zeolitic
362 imidazolate framework-derived porous carbon and their corresponding furfural/acetic acid adsorption
363 separation performance, Chemical Engineering Journal, 428 (2022) 132016.
364 [26] J. Xie, Y. Cao, D. Jia, Enhanced photocatalytic oxidizing ability via adjusting the band-edge
365 position and oxygen defect concentration of bismuth phosphate, Journal of Alloys and Compounds,
366 832 (2020) 154953.

[27] X. Zheng, J. Wang, J. Liu, Z. Wang, S. Chen, X. Fu, Photocatalytic degradation of benzene over different morphology BiPO4: revealing the significant contribution of high–energy facets and oxygen vacancies, Applied Catalysis B: Environmental, 243 (2019) 780-789.

[28] B. Shi, H. Yin, T. Li, J. Gong, S. Lv, Q. Nie, Synthesis of surface oxygen-deficient BiPO4 nanocubes with enhanced visible light induced photocatalytic activity, Materials Research, 20 (2017) 619-627.

[29] Y. Zhu, Q. Ling, Y. Liu, H. Wang, Y. Zhu, Photocatalytic performance of BiPO4 nanorods adjusted via defects, Applied Catalysis B: Environmental, 187 (2016) 204-211.

[30] A.B. Azzam, S. El-Sheikh, R. Geioushy, BA. Salah, M. Farida, ASS Helal, Facile fabrication of a novel BiPO 4 phase junction with enhanced photocatalytic performance towards aniline blue degradation, RSC advances, 9 (2019) 17246-17253.

[31] Y. Guo, P. Wang, J. Qian, Y. Ao, C. Wang, J. Hou, Phosphate group grafted twinned BiPO4 with significantly enhanced photocatalytic activity: Synergistic effect of improved charge separation efficiency and redox ability, Applied Catalysis B: Environmental, 234 (2018) 90-99.

[32] Y. Zhu, Y. Liu, Y. Lv, Q. Ling, D. Liu, Y. Zhu, Enhancement of photocatalytic activity for BiPO 4 via phase junction, Journal of Materials Chemistry A, 2 (2014) 13041-13048.

[33] Y. Wang, Z. Qiang, W. Zhu, W. Yao, S. Tang, Z. Yang, J. Wang, J. Duan, C. Ma, R. Tan, BiPO4 Nanorod/Graphene Composite Heterojunctions for Photocatalytic Degradation of Tetracycline Hydrochloride, ACS Applied Nano Materials, 4 (2021) 8680-8689.

[34] Y. Naciri, A. Hsini, Z. Ajmal, J. Navío, B. Bakiz, A. Albourine, M. Ezahri, A. Benlhachemi, Recent progress on the enhancement of photocatalytic properties of BiPO4 using π–conjugated materials, Advances in colloid and interface science, 280 (2020) 102160.

[35] S. Kumar, P. Karfa, K.C. Majhi, R. Madhuri, Photocatalytic, fluorescent BiPO4@ Graphene oxide based magnetic molecularly imprinted polymer for detection, removal and degradation of ciprofloxacin, Materials Science and Engineering: C, 111 (2020) 110777.

[36] A.B. Azzam, R. Djellabi, S.M. Sheta, S. El-Sheikh, Ultrafast conversion of carcinogenic 4-nitrophenol into 4-aminophenol in the dark catalyzed by surface interaction on BiPO 4/gC 3 N 4 nanostructures in the presence of NaBH 4, RSC Advances, 11 (2021) 18797-18808.

[37] R. Djellabi, M. Ghorab, G. Cerrato, S. Morandi, S. Gatto, V. Oldani, A. Di Michele, C. Bianchi, Photoactive TiO2–montmorillonite composite for degradation of organic dyes in water, Journal of Photochemistry and Photobiology A: Chemistry, 295 (2014) 57-63.

[38] V. Nithya, B. Hanitha, S. Surendran, D. Kalpana, R.K. Selvan, Effect of pH on the sonochemical synthesis of BiPO4 nanostructures and its electrochemical properties for pseudocapacitors, Ultrasonics sonochemistry, 22 (2015) 300-310.

[39] A. Ahmed, Y. Chaker, E.H. Belarbi, O. Abbas, J. Chotard, H. Abassi, A.N. Van Nhien, M. El Hadri, S. Bresson, XRD and ATR/FTIR investigations of various montmorillonite clays modified by monocationic and dicationic imidazolium ionic liquids, Journal of Molecular Structure, 1173 (2018) 653-664.

[40] V.-P. Dinh, P.-T. Nguyen, M.-C. Tran, A.-T. Luu, N.Q. Hung, T.-T. Luu, H.T. Kiet, X.-T. Mai, T.-B. Luong, T.-L. Nguyen, HTDMA-modified bentonite clay for effective removal of Pb (II) from aqueous solution, Chemosphere, 286 (2022) 131766.

[41] P. Chand, A. Joshi, S. Saini, S. Lal, Sol-Gel Assisted Morphology and Phase Dependent Electrochemical Performance of BiPO4 Nanostructures for Energy Storage Applications, Journal of Alloys and Compounds, (2021) 163315.

[42] X. Wang, Y. Ren, Y. Li, G. Zhang, Fabrication of 1D/2D BiPO4/g-C3N4 heterostructured photocatalyst with enhanced photocatalytic efficiency for NO removal, Chemosphere, 287 (2022) 132098.

[43] H. Ye, H. Lin, J. Cao, S. Chen, Y. Chen, Enhanced visible light photocatalytic activity and mechanism of BiPO4 nanorods modified with AgI nanoparticles, Journal of Molecular Catalysis A: Chemical, 397 (2015) 85-92.

417 [44] N. Shaham-Waldmann, Y. Paz, Beyond charge separation: The effect of coupling between
418 titanium dioxide and CNTs on the adsorption and photocatalytic reduction of Cr (VI), Chemical
419 engineering journal, 231 (2013) 49-58.
420 [45] C. Langford, M. Izadifard, E. Radwan, G. Achari, Some observations on the development of
421 superior photocatalytic systems for application to water purification by the “adsorb and shuttle” or
422 the interphase charge transfer mechanisms, Molecules, 19 (2014) 19557-19572.

423